Iran University of Science and Technology

Automotive Science and Engineering

Journal Homepage: ase.iust.ac.ir

ISSN: 2008-9899

Dynamic simulation and performance assessment of a novel powertrain system using liquid ammonia ICE and PEM fuel cell in real driving cycles

Hossein Gharaei[1], Pouria Ahmadi[1*], Pedram Hanafizadeh[1]

[1]School of Mechanical Engineering, College of Engineering, University of Tehran, PO. Box 11155-4563, Tehran, Iran

ARTICLE INFO

Article history:

Received: 13 Dec 2020

Accepted: 31 Feb 2021

Published:1 March 2021

Keywords:

Hybrid powertrain system

PEM fuel-cell

Liquid ammonia ICE

Fuel consumption

Standard driving cycle

A B S T R A C T

This paper introduces a novel powertrain system composed of a liquid ammonia internal combustion engine, a dissociation and separation unit, and a PEM fuel cell system developed for vehicular applications. Using a carbon-free fuel for the ICE and producing hydrogen on board for PEMFC use significantly enhance this novel system's environmental effects. The thermodynamic analyses are conducted using EES and MATLAB software. The results show that while this hybrid powertrain system produces 120 kW output power, energy and exergy efficiencies are 45.2% and 43.1%, respectively. The overall exergy destruction rate of the system becomes 237.4 kW.

The fuel consumption, engine speed, and battery state of charge (SoC) analyses are calculated using three driving cycles. These vehicles consume 7.9, 5.7, and 7.7 liters of liquid ammonia per 100 km in FTP-75, NEDC, and HWFET driving cycles, respectively. The battery state of charge differentiation in these three cycles shows the practicality of this novel powertrain system specially in inner-city driving cycles as the battery does not confront any intense decline of SOC to the minimum level. HWFET results show the great dependence of the vehicle on ICE and low PEM fuel cell function, which results in releasing decomposed hydrogen to the environment.

1. Introduction

In today's life, energy has become a vital need to enhance the quality of life and economic growth of all people. Still, it is essential not to damage nature or harm the environment to achieve it [1], [2]. Each country, according to its resources and technology, deploys different criteria to extract energy. Most developed countries prefer renewable, reliable, and accessible energy resources. While developing countries employ affordable and cheap energy resources that may not be environmentally friendly enough to meet global standards[3], [4].

Energy resources are extended from traditional fuels such as coal and oil, which are no longer popular due to their pollution and low efficiency. High-tech, recently invented energy-producing methods, such as tidal energy, solar cells, biofuel energy, and hydropower [5].

*Corresponding Author
Email Address: pahmadi@ut.ac.ir
https://doi.org/10.22068/ase.2021.581

[DOI: 10.22068/ase.2021.581]

Globally, energy production rate has increased during recent years. However, it is essential to note that amount of energy produced from fossil fuels has declined, and these are renewable energy resources such as geothermal, wind, solar and hydro energy that have impressively increased during the last decade. Figure 1 visualizes the energy consumption rate divided by each energy resource. From this figure, it can be understood that although new technologies have employed novel energy production methods, oil and gas are still determinative energy resources [6].

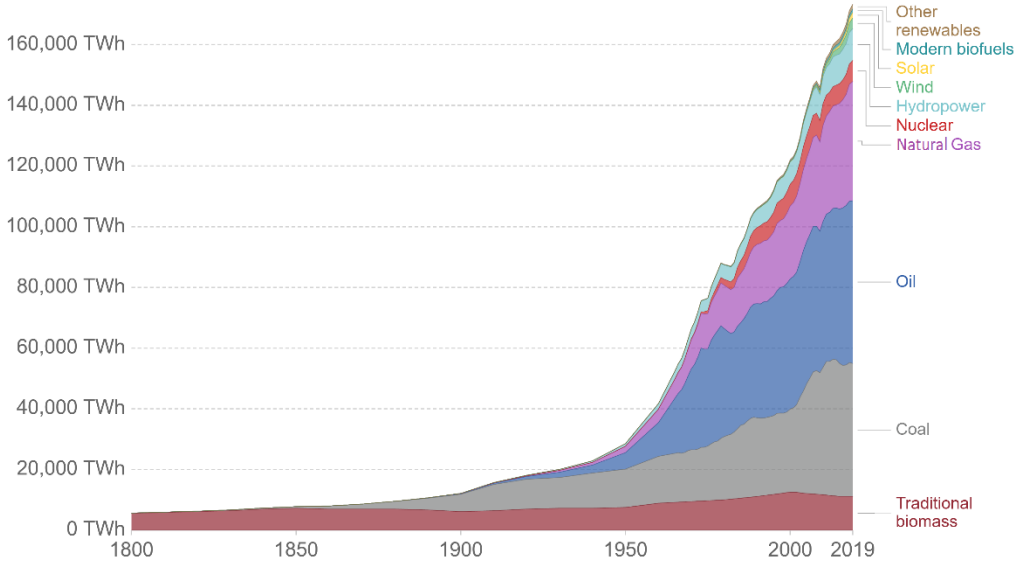

Figure 1: Global energy consumption by source [7]

The infrastructure and financial problems are influential factors that prohibit us from utilizing new energy resources. Also, as mentioned before, the principal energy resources used nowadays are oil, natural gas, and other fossil fuels. So, it is vital to use them more efficiently.

According to the international energy outlook 2016, the transportation sector delivered energy consumption increases at an annual average rate of 1.4%, from 111 EJ in 2012 to 163 EJ in 2040. It is critical to enhancing common fuel usage efficiency to lower energy waste and emitted GHGs. Thus, a novel integrated energy system is designed to be deployed in the transportation system, especially personal vehicles. This hybrid powertrain system is composed of a liquified ammonia ICE and a PEMFC as its primary power sources[8].

Although some novel technologies avoid environmental impacts of present energy-related methods such as chemical looping carbon capture, carbon capture, and storage, these are not long-term efficient solutions. So, it is preferred to alternative fuels such as ammonia and hydrogen to be used instead. Many pieces of research have proved hydrogen preference as an alternative fuel. It can be easily converted into electricity, and it can be produced from renewable materials such as biomass and water. It is also highly environmentally friendly in all processes that it is used. Considering all capabilities of hydrogen, it is a should for novel technologies to benefit from this fuel. It is also crucial that hydrogen can be produced from ammonia decomposition reaction, making it completely compatible with this research's restrictions and design limits [9].

It is preferred for environmental issues to use an alternative fuel such as ammonia in the Internal Combustion Engine. Nowadays, about 85% of worldwide ammonia production uses Haber-Bosch and steam methane reforming processes. Also, ammonia production can be done using renewable energy resources such as wind energy, solar energy, biomass, and hydropower. This vast variety of energy resources can ease ammonia production and make it a sustainable energy resource. Ammonia can be stored in liquid form at a temperature of 25$^{\circ C}$ and pressure of 8.6 atm [10]. As ammonia is a carbon-free fuel, its complete combustion produces just water and nitrogen gas, which is environment-friendly. The combustion of pure ammonia produces a flame with a relatively low propagation speed. This low combustion rate of ammonia causes combustion to be inconsistent and unfavorable. It is usual to add combustion promoters to enhance the combustion properties of liquid ammonia.

[DOI: 10.22068/ase.2021.581]

Ammonia usage as a fuel was first implemented during world war II due to insufficient fossil fuel to run the fleet. Many researchers have studied ammonia usage in ICEs. For example, Grannell et al. [11] used a mixture of ammonia and gasoline to fuel a SI ICE. They understood that pure ammonia caused poor engine performance while mixing 70% ammonia with 30% gasoline using an engine with a 10:1 compression ratio resulted inadequate engine power. Ryu et al. [12] also worked on ammonia-gasoline blended fuel, which is combusted in an ICE using direct injection technology. The study is consisted of comparing this engine with a SI engine running only on gasoline with different injection timings and durations. Frigo and Gentili [13] studied the effect of hydrogen as a promoter for an ammonia ICE. The results showed a remarkable improvement in ignition characteristics and increased velocity of combustion. Mørch et al. [14] investigated combustion characteristics with different ammonia and hydrogen mixture ratios. They concluded that adding 10% of hydrogen by volume or 1% of hydrogen by mass to ammonia fuel makes the fuel considerably enhanced, and the output power and efficiency of the intended engine is increased significantly. Ezzat and Dincer [15] incorporated an ICE running on liquid ammonia, a thermoelectric generator (TEG) and an ammonia electrolyte cell. The results showed that the studied system has an energetic efficiency of 31%, and the ICE has the maximum exergy destruction rate among other components.

Due to its high power-density, instant startup time, and safe and straightforward structure, Proton exchange membrane fuel cell technology is a prime candidate for vehicular and other mobile applications. Hu and Wang et al. [16] achieved semi-empirical equations to model PEMFC operation. PEMFCs are sensitive to the water content of the membrane, and in case of dehydration or flooding, the PEMFC losses its efficiency and power.

Hydrogen that is used in PEMFC can be generated onboard utilizing the process of ammonia thermal decomposition. As this process is endothermic, ICE's high-temperature exhaust gases can be used to supply the hydrogen production process energy. According to Liu et al. [17], This decomposition can occur using a solid nano-sized Ni/SBA-15 catalyst at 650$^{\circ C,}$ which gives 99.2% conversion efficiency. Ammonia normally starts to crack at temperatures of 200$^{\circ C,}$ and as the temperature increases, the decomposition process's efficiency also increases. At 425$^{\circ C,}$ ammonia is decomposed with 98-99% conversion efficiency [18], and at temperatures above 500$^{\circ C}$ there is no need for any catalysts for this process [19]. Kojima et al. [20] filed a patent that hydrogen is produced onboard using the heat of internal combustion engine exhaust gasses. This hydrogen is stored so that it can be used with ammonia to enhance combustion characteristics in the ammonia ICE.

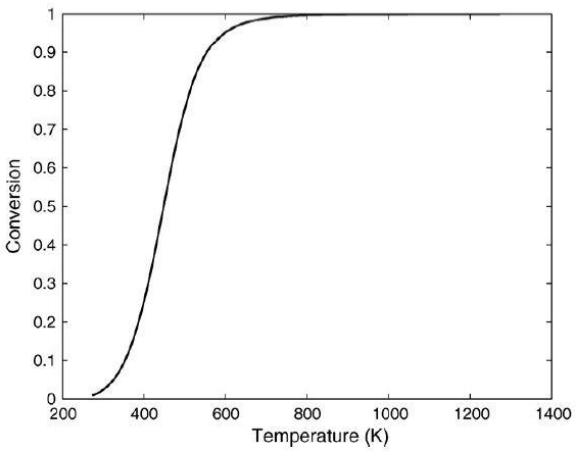

Figure 2: DSU conversion efficiency as a function of temperature[21]

Dincer and Zamfirescu [22] established a new system using Dissociation and separation units of ammonia to produce hydrogen with ammonia for combustion usage. Frigo et al. [18] and Ryu et al. [20] assured that the addition of hydrogen to the ammonia-air mixture makes the combustion faster, and also it lowers fuel consumption and exhaust emission. Besides, the ICE achieves higher output power and performance.

2. Approach

In this study, a novel powertrain system is designed basically for vehicular applications. As it is evident from figure 3, a liquid ammonia tank is used as our primary fuel storage, which operates at 20$^{\circ C}$ and 10atm, the liquid ammonia is used for two purposes; first, the fuel stream of ICE, and the other is the stream of ammonia which is used in DSU to produce hydrogen on board. The products of DSU are nitrogen gas, which will be released to the environment, and hydrogen gas, which is used in the PEMFC unit of our hybrid powertrain system.

The power produced from two sources will provide the vehicle with the power of 120 KW. The powertrain system uses a parallel hybrid design to supply the vehicle with instant power from each of the power units. The hydrogen production system is composed of a DSU functioning with a conversion efficiency of nearly 99% at a temperature of 800K. Supplementary

[DOI: 10.22068/ase.2021.581]

data of DSU is given in table 1. Also, a hydrogen purification unit (HPU) is used following the DSU and before the PEMFC to remove any impurity (ammonia) from the FC system's hydrogen stream. This impurity can cause major failures to the PEMFC and decrease fuel cell output power and efficiency.

The ICE is fueled with a mixture consisted of 99% liquid ammonia and 1% hydrogen by mass. The engine is a spark ignition and 4-stroke engine generating the maximum power of 59KW. The exhaust gases are used in the DSU system to decompose ammonia into hydrogen and nitrogen. Finally, the PEMFC is connected to a battery to store the excess amount of energy. This energy can be supplied to the car's accessories such as air conditioning system, cooling system pumps, and the electric motor to run the vehicle.

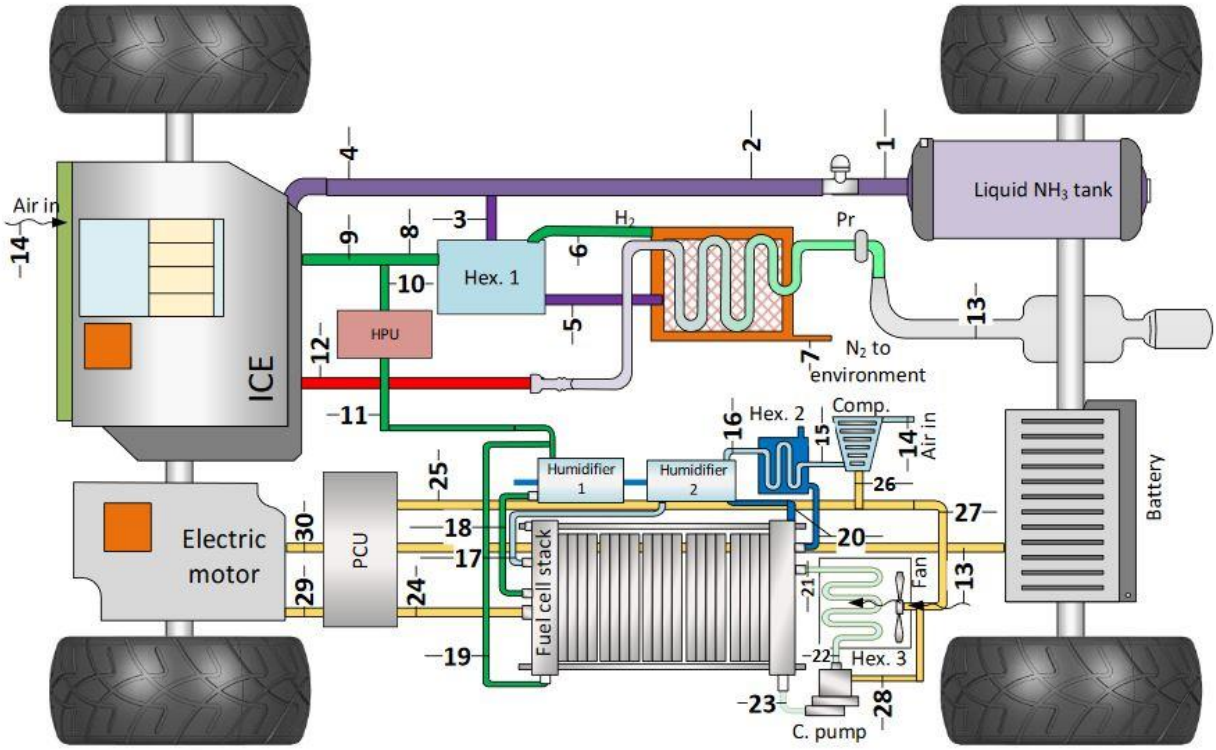

Figure 3: Schematic of the intended powertrain system

3. Modeling

The hybrid powertrain system is modeled in EES, MATLAB, and SimCenter AMESim. The results of thermodynamic analyses consist of energy, exergy efficiencies, and exergy destruction rate analyses. The thermodynamic analyses are used to model the system in SimCenter AMESim to conclude the vehicle fuel consumption, ICE load, and battery state of charge in different driving cycles.

The following assumptions are made for system evaluation and thermodynamic analysis of the system:

- Ambient temperature T_0 and pressure P_0 are considered to be 298 K and 101.325 kPa, respectively.
- Potential and kinetic exergies all assumed to be the same in all states.
- The humidifiers used in the PEMFC system will set the relative humidity of hydrogen and air inlet streams to 90%.
- Except for the pressure regulator, there are no other pressure drops in the system.
- The energy efficiency of the liquid ammonia ICE is considered to be 30%.
- The heat generated from the FC stack is rejected to the surrounding. 80% of this heat is achieved by the fuel cell cooling system, and the 20% rest of it is expelled to the surrounding by radiation and convection.
- For the thermodynamic analysis, the hybrid power train system has a maximum output of 120 kW.
- Fuel cell system accessories such as cooling pumps, fan, and compressor operate adiabatically with an isentropic efficiency of 85%.

[DOI: 10.22068/ase.2021.581]

The total exergy of the flow in each section is calculated according to the formulas given below:

$ex_{total} = ex_{ph} + ex_{ch} + ex_{ke} + ex_{pe}$	(1)
$ex_{ph} = (h - h_0) + T_0(s - s_0)$	(2)
$ex_{ch} = \sum \mu_i^* - \mu_{i,0}$	(3)
$ex_{ch,gas\ mixture} = \sum y_i ex_i^{ch} + RT_0 \sum y_i lnY_i$	(4)

3.1. Pressure regulator analysis

Fuel can easily be stored in a liquid form easily; the fuel tank of this vehicle operates at a temperature and pressure of 293 K and 10 atm, respectively. A pressure regulator is used to decrease the fuel line pressure entering the ICE. The operating pressure of the regulator is 2 atm, and it works adiabatically.

The governing equations and assumptions of the pressure regulator are as below:

$$\begin{cases} T_1 = 293\ K \\ P_1 = 10\ atm \\ P_2 = 2\ atm \\ h_2 = h_1 \end{cases} \quad (4)$$

3.2. Internal combustion engine analysis

The ICE is fueled with ammonia; for enhancing the combustion characteristic, hydrogen gas is used as the promoter, and it is used with a mass ratio of 1% to 99%. The stoichiometric combustion reaction of hydrogen gas and ammonia is as follow [23]:

$$NH_3 + 0.75(O_2 + 3.76N_2) \rightarrow 1.5\ H_2O + 3.32\ N_2 \quad (5)$$

$$H_2 + 2.38\ (0.21\ O_2 + 0.79\ N_2) \rightarrow H_2O + 1.88\ N_2 \quad (6)$$

The ICE is considered to convert 30% of total reactant energy to useful mechanical work, 30% to energy waste from exhaust gases, 30% to energy waste by heat conduction and convection to the cooling system or surrounding, and 10% of total energy is wasted due to lubrication and friction.

The mass balance, energy balance, and exergy balance of the ICE are expressed as the following equations:

$$\dot{m}_4 + \dot{m}_9 + \dot{m}_{14} = \dot{m}_{12} \quad (7)$$

$$\dot{N}_4 h_4 + \dot{N}_9 h_9 + \dot{N}_{14} h_{14} = \dot{N}_{12} h_{12} + \dot{W}_{ICE} + \dot{Q}_{cool} + \dot{Q}_{lub} \quad (8)$$

$$\dot{N}_4 ex_4 + \dot{N}_9 ex_9 + \dot{N}_{14} ex_{14} = \dot{N}_{12} ex_{12} + \dot{W}_{ICE} + \dot{ex}^Q_{cool} + \dot{ex}^Q_{lub} + E\dot{X}d_{ICE} \quad (9)$$

Here the term "$\dot{W}_{ICE}$" is the obtainable power from the ICE, the term."$\dot{Q}_{cool}$" is the heat rejected to the cooling system and the term."$\dot{Q}_{lub}$" is energy loss of lubrication system and friction. Also, in the last equation, the term "$E\dot{X}d_{ICE}$" is exergy destruction rate of ICE.

3.3. Decomposition and separation unit (DSU) analysis

The decomposition of ammonia is an endothermic reaction. The conversion efficiency is a function of temperature. Here the reaction equation can be expressed as below, using dissociation fraction."X_d"[24]:

$$NH_3 \rightarrow 1.5\ X_d\ H_2 + 0.5\ X_d\ N_2 + (1 - X_d)\ NH_3 \quad (10)$$

The heat required for this equation is calculated using the equation given below:

$$\Delta h_{DSU}(T) = h(T) - h_0(T) + X_d * \eta_d * \Delta h_D(T) \quad (11)$$

Here, "Δh_D"The amount of energy required for dissociation reaction of ammonia at temperature T and other standard state conditions. Also, the term "η_d" is the conversion efficiency of the thermal decomposition process[25].

General operating conditions of DSU, used for calculating the required heat of decomposing ammonia, are presented in table 1.

Table 1: DSU general features

Standard enthalpy of reaction	45.9 (kJ/mol)

[DOI: 10.22068/ase.2021.581]

DSU operating temperature	800 k
Ammonia decomposition reaction	$NH_3 \rightarrow 1.5\ H_2 + 0.5\ N_2$
Dissociation factor (X_d)	99.8%
Conversion efficiency (η_d)	1

3.4. Proton exchange membrane fuel cell (PEMFC) analysis

In PEMFCs, the fuel (hydrogen, H_2) enters at the anode. A chemical reaction causes the hydrogen molecules to separate into positive hydrogen ions (H^+ or protons) and electrons (e^-). This reaction releases heat. The positive hydrogen ions pass through the electrolyte made of a polymer membrane and travel to the cathode. The electrons remain behind and thereby give the anode a negative charge, creating a voltage difference between the anode and the cathode. Because electrons travel from negative to positive, the electrons follow an external circuit from the anode to the cathode. Simultaneously, oxygen (O_2) enters the fuel cell at the cathode and combines with the electrons, which have traveled through the external circuit, and the positive hydrogen ions, which have traveled through the electrolyte, to produce water (H_2O) at the cathode. The chemical reactions are represented here [26]:

$$2H_2 \rightarrow 4H^+ + 4e^- \quad (12)$$

$$O_2 + 4H^+ + 4e^- \rightarrow 2H_2O \quad (13)$$

Moreover, the total reaction of a PEMFC is:

$$2H_2 + O_2 \rightarrow H_2O \quad (14)$$

Each cell of the fuel cell can produce 0.7 V voltage. The overall voltage and current can be determined using the parallel and series equivalent circuit of cells.

The cell total output voltage is determined from the equation below [27]:

$$E(i) = E_{Nernst} + \eta_{act} + \eta_{ohmic} + \eta_{diff} \quad (15)$$

The term demonstrates the reversible potential of a cell."E_{Nernst}" and is calculated using the Nernst equation [28], [29]:

$$E_{Nernst} = 1.229 - 8.5 \times 10^{-4}(T - 298.15) + 4.3085 \times 10^{-5} T \left\{\ln\left(p^*_{H_2}\right) + 0.5 \ln\left(p^*_{O_2}\right)\right\} \quad (16)$$

Here "T" is the cell temperature and the terms."$p^*_{H_2}$" and "$p^*_{O_2}$" are partial pressures of hydrogen and oxygen which are involved in the reaction.

The potential losses have consisted of three terms. First, the activation losses are caused by the slowness of the reactions taking place on the electrode surface, and this potential loss is determined using the following equations:

$$\eta_{act} = \eta_{act,a} + \eta_{act,c} \quad (17)$$

$$\eta_{act,a} = -\frac{\Delta G_{ec}}{2F} + \frac{RT}{2F}\ln\left(4FAK^0_a C^*_{H_2}\right) - \frac{RT}{2F}\ln(i) \quad (18)$$

$$\eta_{act,c} = \frac{RT}{a_c zF}\left[ln\left(FAK^0_c \exp\left(\frac{-\Delta G_e}{RT}\right)\left(C^*_{O_2}\right)^{1-a_c}\left(C^*_{H^+}\right)^{a_c}\right) - \ln(\mathrm{i})\right] \quad (19)$$

Here z=1 is the equivalent number of cathode reactions.

These equations can be estimated using semi-empirical constants as below:

$$\eta_{act} = \beta_1 + \beta_2 T + \beta_3 T ln\left(C^{interface}_{O_2}\right) + \beta_4 T ln(I) \quad (20)$$

$$\beta_1 = \left(\frac{-\Delta G_e}{a_c zF}\right) + \left(\frac{-\Delta G_{ec}}{2F}\right) \quad (21)$$

$$\beta_2 = \frac{R}{a_c zF}\ln\left[zFAk^0_c\left(C^*_{H^+}\right)^{1-a_c}\left(C^*_{H_2O}\right)^{a_c}\right] + \frac{R}{2F}\left[\ln\left(4FAK^0_a C^*_{H_2}\right)\right] \quad (22)$$

$$\beta_3 = \frac{R}{a_c zF}(1 - a_c) \quad (23)$$

$$\beta_4 = -\left(\frac{R}{a_c zF} + \frac{R}{2F}\right) \quad (24)$$

These constants are calculated for different operating conditions. Fowler et al. [30] and

[DOI: 10.22068/ase.2021.581]

Maxoulis et al. [31] calculated the values for the coefficients, and these coefficients become:

$$\beta_1 = -0.951 \quad (25)$$

$$\beta_2 = 0.00312 \quad (26)$$

$$\beta_3 = 7.4 \times 10^{-5} \quad (27)$$

$$\beta_4 = -0.000187 \quad (28)$$

The second potential loss considered in the total cell potential equation is ohmic losses. It occurs because of resistance to ions in the electrolyte and resistance to electrons' flow through the electrically conductive fuel cell components. The ohmic loss formula is as below:

$$\eta_{ohmic} = iR^{internal} \quad (29)$$

Here the term "$R^{internal}$" is total resistance, and it has a complicated relation with temperature and pressure and is described as below:

$$R^{internal} = \frac{r_M l}{A} \quad (30)$$

Where "r_M" is Nafion membrane resistance and is calculated according to the equation below:

$$r_m = \frac{181.6\left[1 + 0.03(i) + 0.062\left(\frac{T}{303}\right)^2 i^{2.5}\right]}{[13.366 - 3i]\exp\left(\frac{4.18(T-303)}{T}\right)} \quad (31)$$

The last potential loss term is the diffusion overpotential, it occurs when the rate of mass transport of a species to or from the electrode limits current production, and it is calculated as follow:

$$\eta_{diff} = m\exp(ni) \quad (32)$$

Here "m" correlates to the electrolyte conductivity, and "n" is related to the porosity of the gas diffusion layer. The mass transfer coefficient "m" has two slopes considering fuel cell temperature. This value is presented as:

$$m = 1.1 \times 10^{-4} - 1.2 \times 10^{-6}(T - 273.15) \quad for\ T \geq 312.5k \quad (33)$$

$$m = 3.3 \times 10^{-3} - 8.2 \times 10^{-5}(T - 273.15) \quad for\ T < 312.5 \quad (34)$$

The total power produced by the fuel cell stack is the summation of each cell's power, which can be calculated using the formula below:

$$\dot{W}_{cell} = I \times E(i) \times A_{cell} \quad (35)$$

So, the total power is:

$$\dot{W}_{total} = n_{FC} \times \dot{W}_{cell} \quad (36)$$

Here "n_{FC}" is the cell number in the fuel cell stack.

3.5. AMESim modeling

In this study, AMESim software is used because of its compatibility for modeling novel systems and benefiting from powerful libraries. Three libraries are used to model the intended powertrain system, IFP-drive, fuel cell, and vehicle dynamics [32].

The vehicle dynamic library is used to impose different ambient conditions, driving forces, the elevation of the road, and vehicle input data. Also, more than ten different standard driving cycles are available to be used in this library. In this software, the driver component is selected according to the transmission type that is used. In this study, a 5-speed manual gearbox and a driver component compatible with this transmission type, which commands the gear number, brake pedal usage percentage, and throttle pedal usage percentage, are used.

To model the ICE used in our powertrain case study system, the conventional engine component available in the library is used. Still, it is edited by applying an ammonia ICE characteristic to a 4-stroke engine and imposing related changes to the ECU, fuel properties, and exhaust emissions. On the other hand, the PEM fuel cell is used as the secondary power source with a parallel hybrid design. PEMFC charges a high-capacity battery to be used in case of need [33].

[DOI: 10.22068/ase.2021.581]

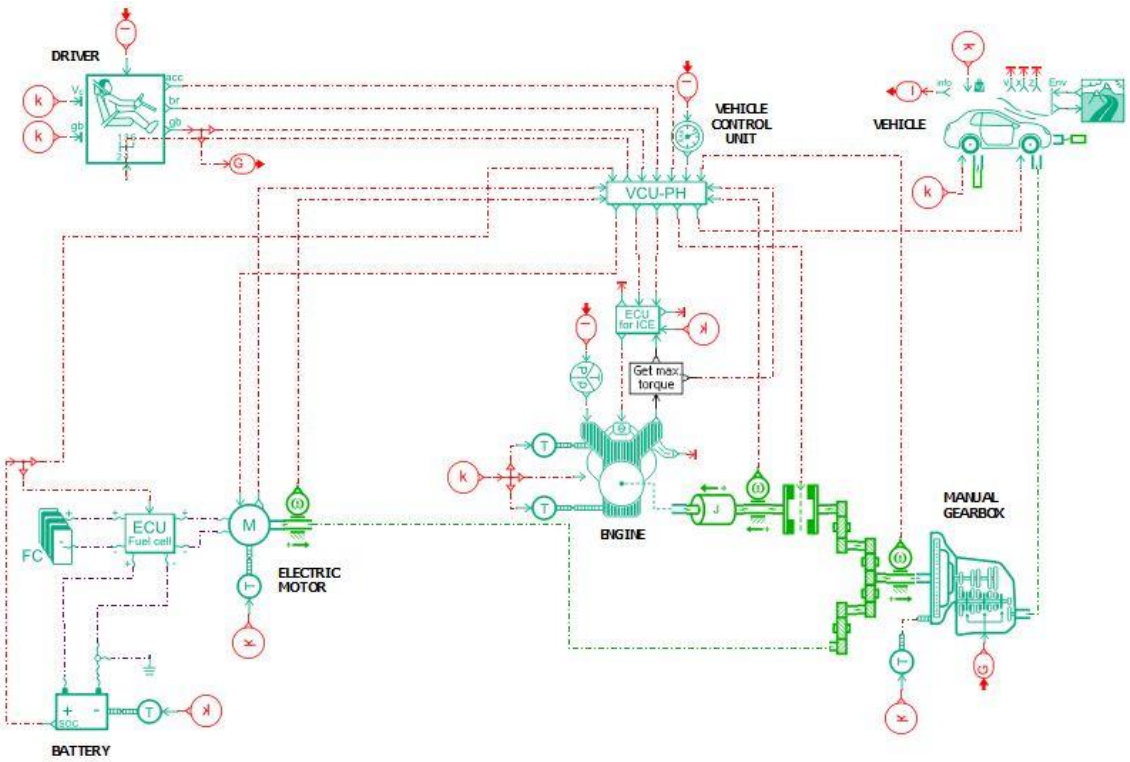

Figure 4: The designed model of the powertrain system in AMESim software

4. Results

The results of the thermodynamic analyses are driven using EES software. Input variables that are used in these analyses are presented in table 2.

Table 2:Iinput variables of thermodynamic analysis (EES and MATLAB)

Variables	Value
Ambient temperature	25^{oC}
Ambient pressure	1 atm
PEMFC maximum power	59 kW
PEMFC current density	1150 mA/cm^2
Cell area	900 cm^2
Cell number	130
FC membrane thickness	0.183 mm
FC operating pressure	2 atm
FC operating temperature	50^{oC}
Hydrogen stoichiometry	1.2
Oxygen stoichiometry	2
Air inlet humidity	0.9
Hydrogen inlet humidity	0.9
ICE maximum output power	59 kW
Hydrogen LHV	240 kJ/mol
Oxygen LHV	314.5 kJ/mol
Fuel tank pressure	10 atm
Fuel tank temperature	20^{oC}
Hydrogen to ammonia mass ratio	0.01
DSU efficiency	0.9
Fan and compressor efficiency	0.85
ICE efficiency	0.3
DSU operating temperature	800 K

[DOI: 10.22068/ase.2021.581]

In this study, as is shown in figure 5, the influence of changing hydrogen to ammonia mass ratio on ICE output power is considered. This figure clearly states that by increasing the hydrogen ratio from 0% to 5 %, the ICE power is increased by 21%, but this ratio change's primary concern is the combustion characteristics. As indicated previously, pure ammonia does not combust steadily and has low flammability. So, we add 1% hydrogen by mass to achieve acceptable combustion properties.

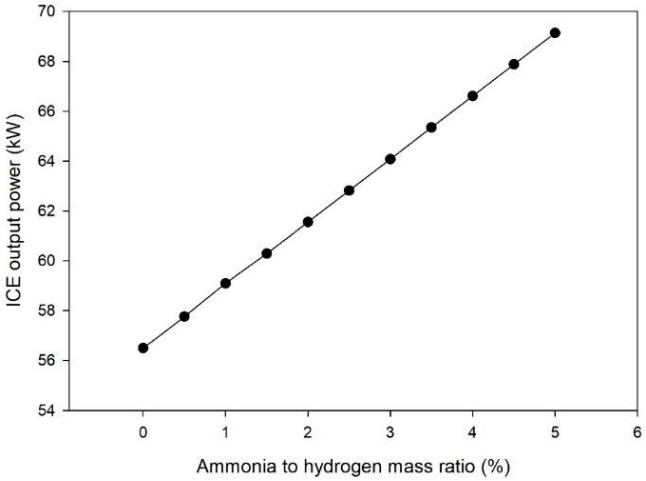

Figure 5: ICE output power as a function of hydrogen to ammonia mass ratio

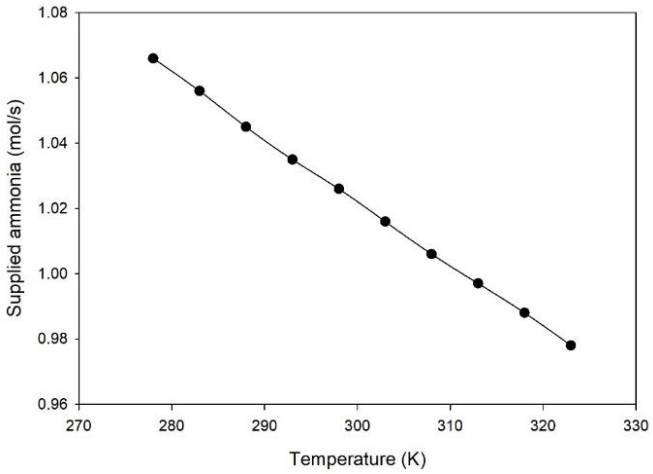

Figure 6: supplied ammonia to the ICE as a function of ambient temperature to achieve 59 kW power

Figure 6 shows that the supplied ammonia to ICE decreases from 1.065 (mol/s) to 0.975 (mol/s) as the ambient temperature increases to 50 degrees centigrade.

As ammonia is used to fuel the ICE, the output power and exergy destruction rate would vary according to the amount of ammonia supplied to the ICE. These variations are demonstrated in figure 7, and it is understood from the figure that they vary linearly with the supplied ammonia amount.

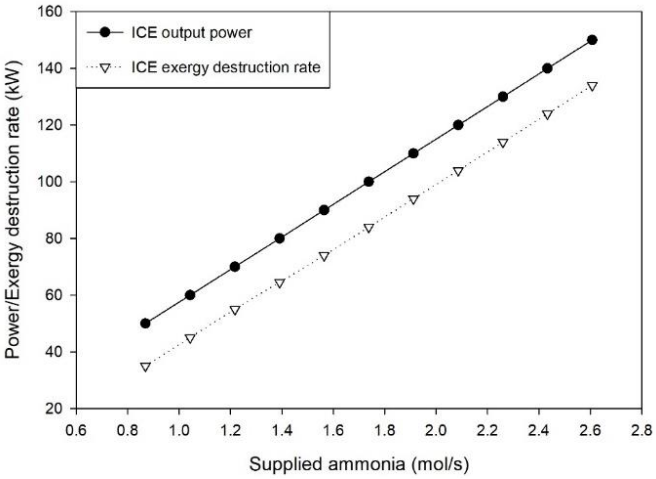

Figure 7: output power and exergy destruction rate according to supplied ammonia to ICE

PEMFC operation strongly depends on the hydrogen production rate of DSU. According to governing equations of DSU, the operating temperature of DSU and heat supplied to this unit are its substantial variables. Also, a sufficient amount of ammonia has to be fed to DSU. Figures 8, 9, and 10 present hydrogen production rate and ammonia decomposition rate as a function of heat applied to DSU, ICE exhaust gas temperature, and DSU operating temperature.

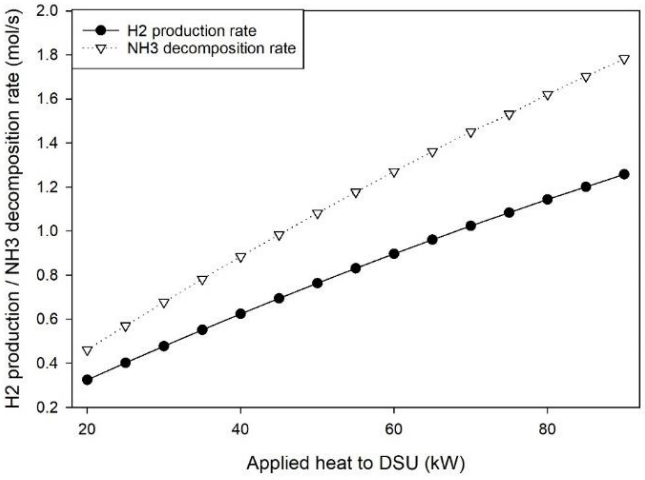

Figure 8: hydrogen production and ammonia decomposition rate as a function of applied heat to DSU

[DOI: 10.22068/ase.2021.581]

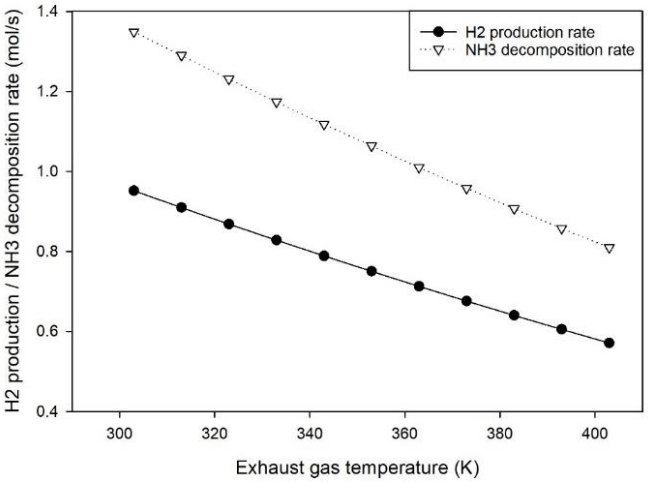

Figure 9 hydrogen production and ammonia decomposition rate as a function of exhaust gas temperature

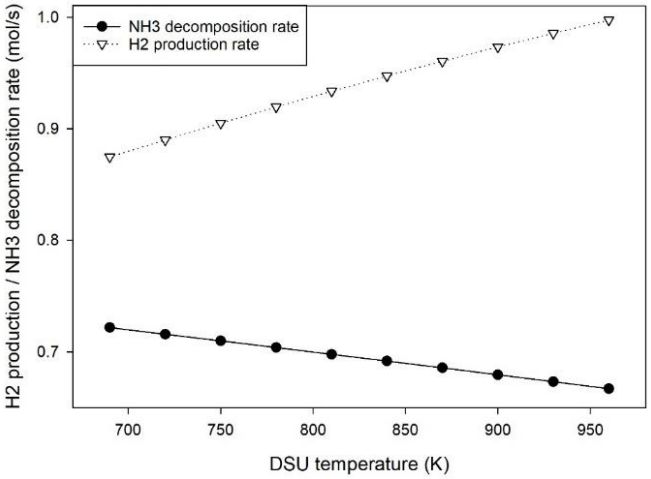

Figure 10:hydrogen production and ammonia decomposition rate as a function of DSU temperature

overall operation of Dissociation and separation unit is discussed in figure 11. It is comprehended from this figure that by increasing the amount of ammonia supplied to the DSU, required heat and recovered exergy increase linearly. However, ammonia consumption rate and hydrogen production rate do not increase linearly, and it would experience a declining trend in production rate.

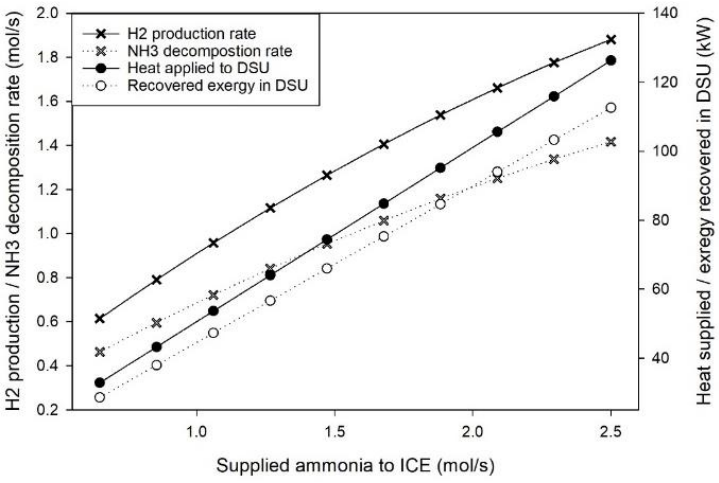

Figure 11: overall performance variation of DSU with the supplied amount of ammonia

In this study, the ICE and PEMFC employed in the powertrain system are principal components whose performance is our specific target of the investigation. As figure 12 indicates, ICE output power increases from 49 kW to 91 KW, PEMFC power increases from 67 kW to 113 kW, proportional to the amount of ammonia supplied to the ICE increases from 0.87 mol/s to 1.66 mol/s. These two components' exergy destruction rate has the same trend as the output power with a ratio of nearly ½.

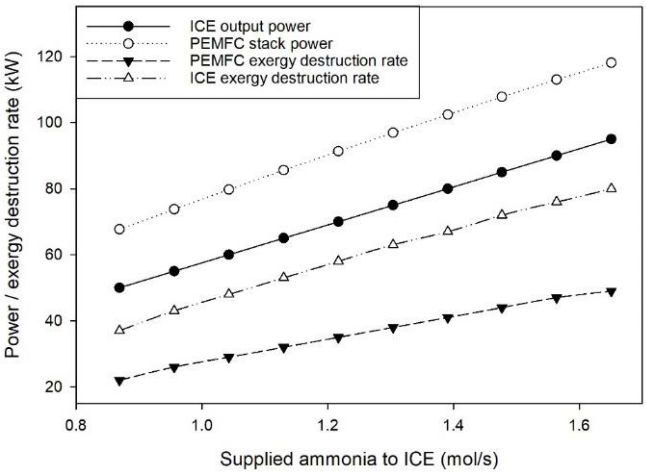

Figure 12:effect of varying supplied ammonia on ICE and PEMFC power and exergy destruction rate

The powertrain system's overall efficiencies are expressed in figure 13. At the assumed power output of 118 kW, the energy efficiency of the system is 44.2%, and the exergy efficiency is 43.1%, which are significantly higher than conventional diesel and petrol engines and make this novel system a capable alternative powertrain system to be used in public transportation and personal vehicles.

[DOI: 10.22068/ase.2021.581]

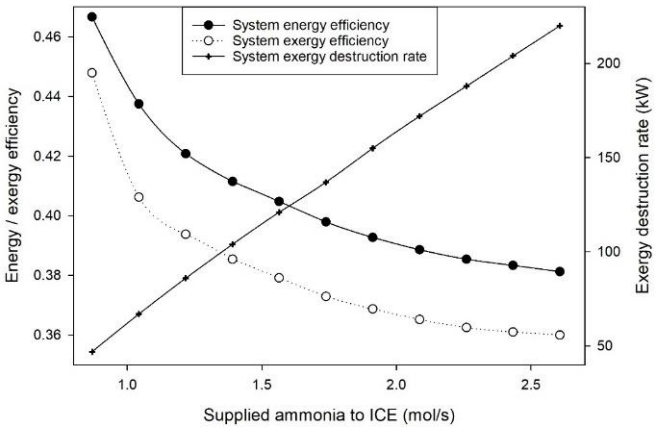

Figure 13: overall powertrain system efficiencies and exergy destruction rate as supplied ammonia varies

The next step is to use the last part's results to model the powertrain system in AMESim software. The input variables are provided in table 3. In this part, 3 different driving cycles are used to conclude fuel consumption, hydrogen usage in PEMFC, battery state of charge, and engine load.

Table 3: input variables for modeling the system in AMESim software

Variables	Value
Vehicle mass	$1400\ kg$
Drag coefficient	0.32
Vehicle frontal area	$2.1\ m^2$
Ambient temperature	25^{oC}
Minimum battery SOC for recharging using engine power	45%
Maximum battery SOC to stop recharging using engine power	90%
Vehicle speed to start hybridization	$10\frac{m}{s}$
Idle engine speed	$700\ rpm$
Maximum engine speed	$6000\ rpm$
ICE displacement	$2.4\ L$
Transmission type	$5-speed\ manual\ gear\ box$
Fuel heat of combustion	$22.5\frac{MJ}{kg}$
Electric motor operating voltage	$144\ V$
Initial battery state of charge	65%

THE first FTP-75 driving cycle is considered in this driving cycle, which is 7.5 km long, the average speed of the vehicle is 11.4 m/s, and 275.9 gr of ammonia is consumed in this cycle. Also, the fuel cell in this driving cycle consumes 32.2 gr of hydrogen dissociated in DSU.

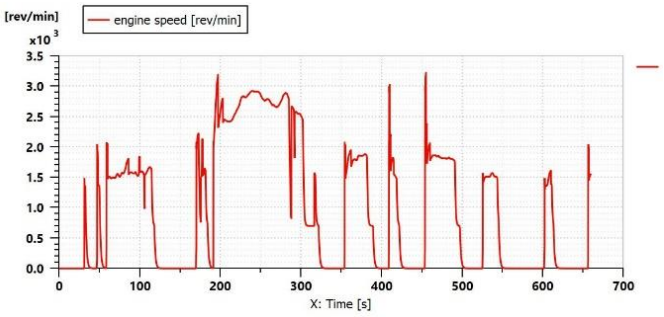

Figure 14: ICE speed in FTP-75 cycle

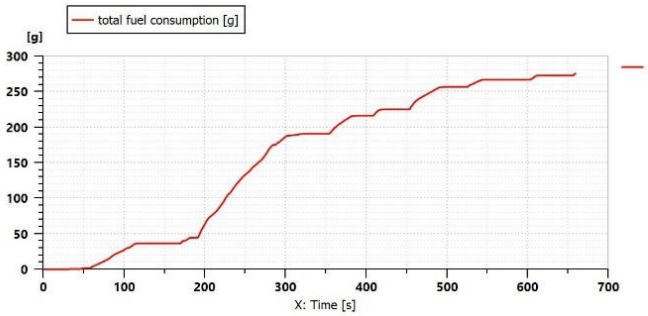

Figure 15: cumulative ammonia consumption in FTP-75 cycle

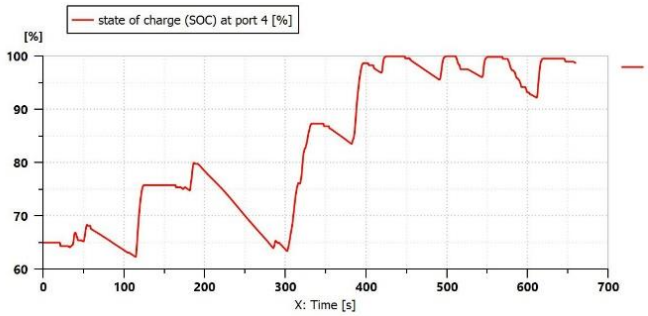

Figure 16: battery SOC in FTP-75 cycle

The second driving cycle studied is NEDC. This cycle is not a realistic driving cycle, and most researchers have criticized it. This driving cycle is 5.9 km long, the average speed is 8.9 m/s, and the proposed vehicle consumes 63.9 gr ammonia and 32.1 gr hydrogen to travel this cycle.

[DOI: 10.22068/ase.2021.581]

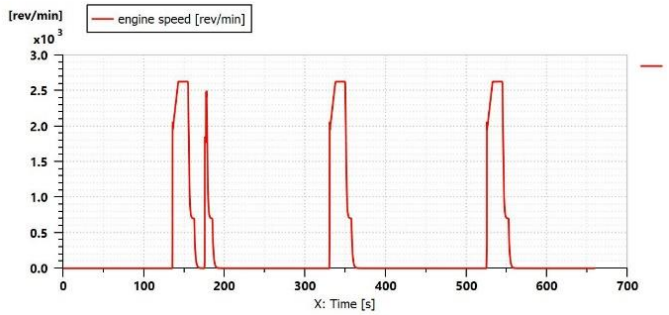

Figure 17: ICE speed in NEDC cycle

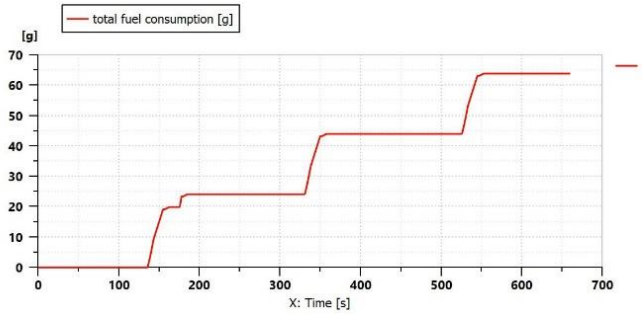

Figure 18: cumulative ammonia consumption in NEDC cycle

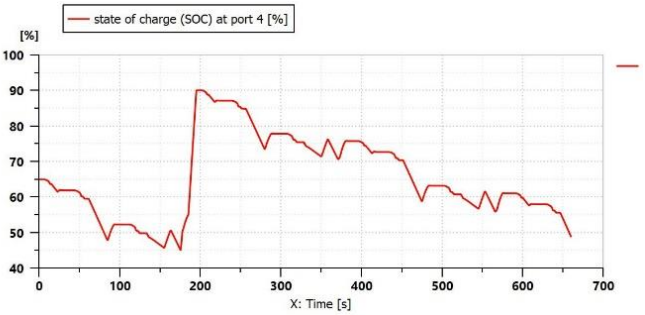

Figure 19: battery SOC in the NEDC cycle

The last driving cycle, which is reviewed in this study, is HWFET or highway driving cycle. This driving cycle is characterized by higher driving speed and longer travel distances than other driving cycles. HWFET is 15 km long, and the average speed to travel this driving cycle is 22.8 m/s. As the vehicle in this cycle runs with higher speed than other cycles, more ammonia is combusted in the ICE, and a lower amount of hydrogen is used in PEMFC. So, the rest of the hydrogen produced in the DSU system should be released into the environment. For this defect of the powertrain system, it is preferred to redesign the vehicle propulsion system to use a hydrogen tank to store the excess hydrogen gas and use it in case of need like this driving cycle.

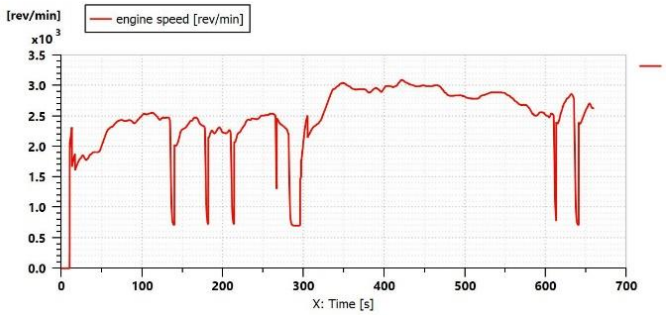

Figure 20: ICE speed in HWFET cycle

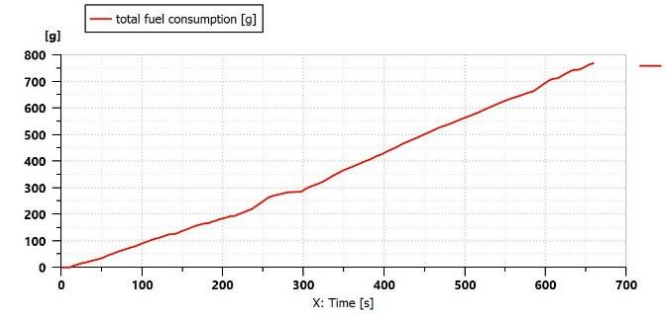

Figure 21: cumulative ammonia consumption in HWFET cycle

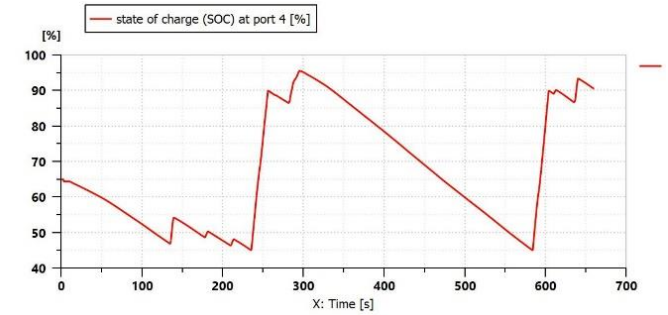

Figure 22: battery SOC in HWFET cycle

4. Conclusions

The thermodynamic analysis results clearly show the severe dependence of output power, hydrogen production rate, and overall efficiencies of the system on the amount of ammonia supplied to the ICE. The results show that for obtaining 60 kW power from the ICE, the ICE should be supplied with 1.1 mol/s ammonia. In this condition, the DSU decomposes 0.77 mol/s ammonia and produce 1.02 mol/s hydrogen gas to be used in the PEMFC. The maximum power of PEMFC in this condition can reach 79 kW, but we limit fuel cell power to 59 KW due to DSU and fuel cell system restrictions and efficiencies to work in real conditions. The overall powertrain system energy and exergy efficiencies in this operating condition are 45% and 43%, respectively. Also, the total exergy destruction rate of the system becomes 237.4 kW.

The next part of the results is dedicated to AMESim modeling. The results show a

[DOI: 10.22068/ase.2021.581]

significant change of results as the initial battery state of charge changes and other variables such as hybridization process activation speed, minimum and maximum battery recharge level, which are so determinative in our final results. The FTP-75 driving cycle results show that the vehicle consumes 36.5 gr/km ammonia and 4.3 gr/km hydrogen. In the NEDC cycle, in which the vehicle is driven with a lower average speed, 10 gr/km ammonia and 4.3 gr/km hydrogen are consumed. Finally, in the highway driving cycle, the combustion engine is the primary power source and consumes 51.2 gr/km. The fuel cell system experiences a very low operation cycle with consuming just 1.2 gr/km hydrogen. These results authenticate the performance of the established powertrain system. The energy and exergy efficiencies of this system are higher than conventional ICE engine despite that the fuel storage and transport infrastructures of this vehicle is feasible with present technologies and equipment

List of symbols (Optional)

A	Cell area
$E(i)$	Total fuel cell voltage
R	Gas constant
F	Faraday constant
P	Pressure
T	Temperature
N	Molar flow rate
I	Current
i	Current density
$C^*_{O_2}$	Oxygen concentration at the cathode
$C^*_{H_2}$	Liquid phase concentration of hydrogen at the cathode
$C^*_{H_2O}$	Water concentration at the cathode
$p^*_{O_2}$	The partial pressure of oxygen
$p^*_{H_2}$	The partial pressure of hydrogen
$R^{internal}$	Total internal resistance
l	Membrane thickness
LHV	Lower heating value
HHV	Higher heating value

Greek symbols

η_{act}	Activation overpotential
η_{ohmic}	Ohmic overpotential
η_{diff}	Diffusion overpotential
λ_{mem}	Membrane water content

[DOI: 10.22068/ase.2021.581]

References

[1] World Energy Council, "2013 Survey: Summary," p. 29, 2013.

[2] M. Finley, G. Manager, and G. E. Markets, "BP: statistical review of world energy, June 2010," *Vopr. Ekon.*, vol. 2010, no. 10, pp. 101–112, 2010.

[3] BP, "Statistical Review of World Energy, 2020 | 69th Edition," p. 66, 2020.

[4] "Transportation sector energy consumption," *U.S. Energy Information Administration*, 2016. [Online]. Available: https://cleantechnica.com/2019/05/26/why-every-vehicle-should-have-an-electric-motor-even-if-it-doesnt-have-a-plug/.

[5] "Handbook of Fuels: Energy Sources for Transportation," *Chromatographia*, 2008.

[6] U.S. Department of Energy and Fuel Cell Technologies Office, "Multi-Year Research, Development, and Demonstration Plan," *Annu. Prog. Rep.*, 2016.

[7] B. P. S. Review and W. E. June, "BP Statistical Review of World Energy," no. June, 2015.

[8] J. R. González-Montaña, A. J. Alonso Diez, M. E. Alonso de la Varga, and S. Avila Téllez, "Salud de glándulas mamarias en ovejas, cuantificado por CCS y cultivo bacteriológico de casos positivos a CMT. 'Estudio clínico-zootécnico de caso.' Health of mammary glands in sheep, quantified by CCS and bacteriological culture of CMT positive cases. "A," *XXVII Congr. Int. Ovinocultura. Asoc. Mex. Espec. en ovinocultura*, vol. 2016, pp. 127–137, 2013.

[9] F. Safari and I. Dincer, "A review and comparative evaluation of thermochemical water splitting cycles for hydrogen production," *Energy Conversion and Management*. 2020.

[10] C. Zamfirescu and I. Dincer, "Using ammonia as a sustainable fuel," *J. Power Sources*, 2008.

[11] S. M. Grannell, D. N. Assanis, S. V. Bohac, and D. E. Gillespie, "The fuel mix limits and efficiency of a stoichiometric, ammonia, and gasoline dual fueled spark ignition engine," *J. Eng. Gas Turbines Power*, 2008.

[12] K. Ryu, G. E. Zacharakis-Jutz, and S. C. Kong, "Effects of gaseous ammonia direct injection on performance characteristics of a spark-ignition engine," *Appl. Energy*, 2014.

[13] S. Frigo and R. Gentili, "Analysis of the behaviour of a 4-stroke Si engine fuelled with ammonia and hydrogen," *Int. J. Hydrogen Energy*, 2013.

[14] C. S. Mørch, A. Bjerre, M. P. Gøttrup, S. C. Sorenson, and J. Schramm, "Ammonia/hydrogen mixtures in an SI-engine: Engine performance and analysis of a proposed fuel system," *fuel*, 2011.

[15] M. F. Ezzat and I. Dincer, "Development and assessment of a new hybrid vehicle with ammonia and hydrogen," *Appl. Energy*, 2018.

[16] M. Hu, X. Zhu, M. Wang, A. Gu, and L. Yu, "Three dimensional, two phase flow mathematical model for PEM fuel cell: Part II. Analysis and discussion of the internal transport mechanisms," *Energy Convers. Manag.*, 2004.

[17] H. Liu, H. Wang, J. Shen, Y. Sun, and Z. Liu, "Preparation, characterization and activities of the nano-sized Ni/SBA-15 catalyst for producing COx-free hydrogen from ammonia," *Appl. Catal. A Gen.*, 2008.

[18] R. Lan, J. T. S. Irvine, and S. Tao, "Ammonia and related chemicals as potential indirect hydrogen storage materials," *International Journal of Hydrogen Energy*. 2012.

[19] Q. Ma, R. R. Peng, L. Tian, and G. Meng, "Direct utilization of ammonia in intermediate-temperature solid oxide fuel

[DOI: 10.22068/ase.2021.581]

cells," *Electrochem. commun.*, 2006.

[20] K. Susumu, N. Nakamura, R. Shimizu, T. Sugimoto, and K.-O. Kim, "Ammonia burning internal combustion engine," 2009.

[21] V. Alagharu, S. Palanki, and K. N. West, "Analysis of ammonia decomposition reactor to generate hydrogen for fuel cell applications," *J. Power Sources*, 2010.

[22] Z. C. Dincer I, "Methods and apparatus for using ammonia as sustainable fuel, refrigerant and nox reduction agent," 2011.

[23] G. Ciccarelli, D. Jackson, and J. Verreault, "Flammability limits of NH3-H2-N2-air mixtures at elevated initial temperatures," *Combust. Flame*, 2006.

[24] A. S. Chellappa, C. M. Fischer, and W. J. Thomson, "Ammonia decomposition kinetics over Ni-Pt/Al2O3 for PEM fuel cell applications," *Appl. Catal. A Gen.*, 2002.

[25] S. F. Yin, B. Q. Xu, X. P. Zhou, and C. T. Au, "A mini-review on ammonia decomposition catalysts for on-site generation of hydrogen for fuel cell applications," *Applied Catalysis A: General*. 2004.

[26] O. Z. Sharaf and M. F. Orhan, "An overview of fuel cell technology: Fundamentals and applications," *Renewable and Sustainable Energy Reviews*. 2014.

[27] M. A. R. S. Al-Baghdadi, "Modelling of proton exchange membrane fuel cell performance based on semi-empirical equations," *Renew. Energy*, vol. 30, no. 10, pp. 1587–1599, 2005.

[28] A. Bejan, "Heat transfer, second edition," 1995.

[29] A. Bejan, "The thermodynamic design of heat and mass transfer processes and devices," *Int. J. Heat Fluid Flow*, 1987.

[30] M. W. Fowler, R. F. Mann, J. C. Amphlett, B. A. Peppley, and P. R. Roberge, "Incorporation of voltage degradation into a generalised steady state electrochemical model for a PEM fuel cell," *J. Power Sources*, 2002.

[31] C. N. Maxoulis, D. N. Tsinoglou, and G. C. Koltsakis, "Modeling of automotive fuel cell operation in driving cycles," *Energy Convers. Manag.*, 2004.

[32] R. I. Salim, H. Noura, and A. Fardoun, "The use of LMS amesim in the fault diagnosis of a commercial PEM fuel cell system," *Adv. Sci. Technol. Eng. Syst.*, vol. 3, no. 1, pp. 297–309, 2018.

[33] Y. Zhang, P. Bao, Y. Wan, and S. Xu, "Modeling and analysis of air supply system of polymer electrolyte membrane fuel cell system," *Energy Procedia*, vol. 142, pp. 1053–1058, 2017.

[DOI: 10.22068/ase.2021.581]